Earth and Planetary Science Letters 413 (2015) 37–50

Contents lists available at ScienceDirect

Earth and Planetary Science Letters

www.elsevier.com/locate/epsl

Contribution of enhanced Antarctic Bottom Water formation to Antarctic warm events and millennial-scale atmospheric CO_2 increase

L. Menviel [a,b,*], P. Spence [a,b], M.H. England [a,b]

[a] Climate Change Research Centre, University of New South Wales, Sydney, Australia
[b] ARC Centre of Excellence for Climate System Science, Australia

ARTICLE INFO

Article history:
Received 2 June 2014
Received in revised form 4 December 2014
Accepted 29 December 2014
Available online 14 January 2015
Editor: J. Lynch-Stieglitz

Keywords:
Atlantic Meridional Overturning Circulation
Antarctic Isotope Maximum
bipolar seesaw
atmospheric CO_2
Antarctic Bottom Water

ABSTRACT

During Marine Isotope Stage 3, the Atlantic Meridional Overturning Circulation (AMOC) weakened significantly on a millennial time-scale leading to Greenland stadials. Ice core records reveal that each Greenland stadial is associated with a warming over Antarctica, so-called Antarctic Isotope Maximum (AIM), and that atmospheric CO_2 increases with Antarctic temperature during the long Greenland stadials. Here we perform transient simulations spanning the period 50–34 ka B.P. with two Earth System Models (LOVECLIM and the UVic ESCM) to understand the possible link between changes in the AMOC, changes in high latitude Southern Hemispheric climate and evolution of atmospheric CO_2. We find that oceanic carbon releases due to the AMOC resumption during stadial/interstadial transitions lead to an atmospheric CO_2 increase. However, the atmospheric CO_2 increases observed during the first parts of AIM12 (~47.6 ka B.P.) and AIM8 (~39.8 ka B.P.) occur during periods of weak AMOC (HS5 and HS4 respectively) and could instead be explained by enhanced Antarctic Bottom Water transport. Enhanced Antarctic Bottom Water formation is shown to effectively ventilate the deep Pacific carbon and lead to CO_2 outgassing into the atmosphere. In addition, changes in the AMOC alone are not sufficient to explain the largest Antarctic Isotope Maxima (namely AIM12 and AIM8). Stronger formation of Antarctic Bottom Water during AIM12 and AIM8 would enhance the southern high latitude warming and lead to a better agreement with high southern latitude paleoproxy records. The robustness of this southern warming response is tested using an eddy-permitting coupled ocean sea–ice model. We show that stronger Antarctic Bottom Water formation contributes to Southern Ocean surface warming by increasing the Southern Ocean meridional heat transport.

1. Introduction

During Marine Isotope Stage 3 (MIS3, 59.4–27.8 ka B.P.), Greenland and North Atlantic climate oscillated between stadial and interstadial conditions on a millennial time-scale (Masson-Delmotte et al., 2013), in what are called Dansgaard–Oeschger (DO) cycles. DO cycles are characterized by an abrupt warming of 8 to 15 °C within a few decades in Greenland (Dansgaard et al., 1993; Huber et al., 2006), followed by a gradual cooling and then a Greenland stadial. During some Greenland stadials, named Heinrich stadials (Sánchez-Goñi and Harrison, 2010), thick layers of ice-rafted debris are found in marine sediment cores from the North Atlantic (e.g. Hemming, 2004). Paleoproxy records and modeling studies have suggested that DO cycles and Heinrich stadials were part of a continuum of variability that is generated through ice sheet-driven changes in the Atlantic Meridional Overturning Circulation (AMOC) (e.g. Elliot et al., 1998, 2002; Grousset et al., 2001; Sarnthein et al., 2001; Timmermann et al., 2003; Dokken et al., 2013; Menviel et al., 2014b).

During Greenland stadials cold and dry conditions prevailed over Greenland (Alley, 2000; Huber et al., 2006), the North Atlantic (e.g. Bard, 2002; Martrat et al., 2007) and Europe (e.g. Sánchez-Goñi et al., 2002; Fleitmann et al., 2009; Harrison and Sánchez Goñi, 2010). Concurrently, Antarctic ice cores have revealed that during each Greenland stadial of MIS3, air temperature over Antarctica rose by 1 to 3 °C (EPICA and community members, 2006), in what are called Antarctic Isotope Maxima (AIM)[1] (EPICA and community members, 2006). Marine sediment cores from the Southern Ocean further suggest that the surface of the Southern

* Corresponding author at: Climate Change Research Centre, University of New South Wales, Sydney, Australia.
E-mail address: l.menviel@unsw.edu.au (L. Menviel).

[1] For simplicity, in this manuscript, AIM denotes both the singular maximum and plural maxima.

http://dx.doi.org/10.1016/j.epsl.2014.12.050
0012-821X/

Ocean warmed during the large AIM events (Pahnke et al., 2003; Crosta et al., 2004; Kaiser et al., 2005; Caniupán et al., 2011; Lopes dos Santos et al., 2013).

In contrast to other subtropical basins, under present day conditions the ocean heat transport in the South Atlantic is equatorward due to the presence of a strong AMOC (Perez et al., 2011). Previous studies (Crowley, 1992; Stocker, 1998) suggested that the bipolar seesaw pattern in surface air temperature during AIM was due to heat redistribution in the Atlantic basin: as the AMOC weakens its associated northward heat transport also reduces. In addition, while atmospheric CO_2 increased during the large AIM (e.g. AIM12 and AIM8), little atmospheric CO_2 changes were observed during the small amplitude AIM (e.g. AIM10) (Ahn and Brook, 2008, 2014; Bereiter et al., 2012). It has thus been widely accepted that the Southern Hemispheric warming observed during Greenland stadials was the result of meridional heat transport reorganization due to AMOC changes and due to atmospheric CO_2 increase (e.g. Timmermann et al., 2010).

Idealized experiments featuring a shutdown of the AMOC under constant Last Glacial Maximum boundary conditions have been performed with several coupled Atmosphere–Ocean General Circulation Models. However, not all models display a warming signal over Antarctica and the Southern Ocean (Kageyama et al., 2013) concomitant with an AMOC shutdown. Furthermore, when a surface warming is simulated over Antarctica it is of the order of ∼1 °C (Kageyama et al., 2009; Otto-Bliesner and Brady, 2010; Buiron et al., 2012), which is less than temperature anomaly estimates from Antarctic ice cores for the large AIM (e.g. AIM12 and AIM8) (Brook et al., 2005; Jouzel et al., 2007; Uemura et al., 2012). Finally, it is questionable whether the bipolar seesaw effect (i.e. meridional heat transport reorganization) can explain the duration of the warming observed over Antarctica during AIM12, which is over 1000 yr longer than Heinrich stadial 5 (HS5).

Changes in atmospheric CO_2 observed during MIS3 have been tentatively explained by previous modeling experiments. While some studies suggest that the carbon source to the atmosphere is of terrestrial origin (Scholze et al., 2003; Köhler et al., 2005; Obata, 2007; Menviel et al., 2008; Bozbiyik et al., 2011) others attribute it to an oceanic carbon release (Marchal et al., 1999; Schmittner et al., 2007; Schmittner and Galbraith, 2008; Bouttes et al., 2012; Matsumoto and Yokoyama, 2013). However these studies were very idealized as they were performed from either constant Last Glacial Maximum or pre-industrial conditions and used an idealized freshwater forcing.

Significant uncertainties remain regarding the mechanism leading to the large AIM and their relationship with changes in atmospheric CO_2. Menviel et al. (2014a) recently suggested that a strengthening of Antarctic Bottom Water (AABW) transport during Heinrich stadial 4 (HS4) could release deep Pacific Ocean carbon and lead to an atmospheric CO_2 increase in general agreement with the one recorded in Siple Dome ice core at ∼39.8 ka B.P. (Ahn and Brook, 2014). Here we extend this hypothesis and show that enhanced AABW transport during Heinrich stadials could explain part of the observed changes in high Southern latitude temperature and atmospheric CO_2.

The goal of this study is to better understand the origin of the large AIM, the associated changes in atmospheric CO_2 and their relationship with Greenland stadials. We simulate the sequence of high southern latitude millennial-scale events as well as the atmospheric CO_2 variations during the period 50–34 ka B.P. with two Earth System Models of Intermediate Complexity (LOVECLIM and the UVic ESCM). We use two different Earth System Models to test the robustness of the mechanism leading to high southern latitude warming and changes in atmospheric CO_2.

Given that most of the observed ocean kinetic energy occurs on the mesoscale (10–100 km length scales) (Wunsch, 2007), there is considerable debate surrounding the adequacy of ocean meridional heat transport simulated at coarse resolution, particularly in the Southern Ocean where mesoscale eddies are ubiquitous (Spence et al., 2012; Morrison et al., 2013; Bryan et al., 2014). Therefore, we further investigate the relationship between enhanced AABW formation and SST changes using a global eddy-permitting ocean sea–ice model.

2. Models and experimental setup

2.1. Transient simulations of MIS3 performed with LOVECLIM and the UVic ESCM

LOVECLIM consists of a free surface ocean general circulation model (CLIO) with a horizontal resolution of 3° longitude, 3° latitude and 20 depth layers (Goosse et al., 2010). The atmospheric component (ECBilt) is a spectral T21, three-level model based on quasi-geostrophic equations of motion and ageostrophic corrections. LOVECLIM also includes a dynamic–thermodynamic sea–ice model, a land surface scheme, a dynamic global vegetation model (VECODE) (Brovkin et al., 1997) and a marine carbon cycle model (LOCH) (Mouchet, 2011; Menviel et al., 2008).

The UVic Earth System Climate Model (UVic ESCM v2.9) (Weaver et al., 2001) consists of an ocean general circulation model (Modular Ocean Model, Version 2) with a resolution of 3.6° longitude and 1.8° latitude, coupled to a vertically integrated two dimensional energy-moisture balance model of the atmosphere including a parameterization of geostrophic wind stress anomalies, a dynamic–thermodynamic sea–ice model, a land surface scheme, a dynamic global vegetation model, a marine carbon cycle model (Schmittner et al., 2008). Sediment processes are represented using an oxic model of sediment respiration (Archer, 1996; Eby et al., 2009). The oceans barotropic momentum equations are solved with a rigid lid formulation and surface freshwater fluxes are converted to fluxes of salt with a constant salt to freshwater mass ratio of 3.49×10^{-2}.

Initial conditions for both LOVECLIM and the UVic ESCM were obtained by conducting a 15,000 yr equilibrium spin-up simulation using an atmospheric CO_2 content of 207.5 ppmv, orbital forcing for the time 50 ka B.P. and an estimate of the 50 ka B.P. ice sheet orography and albedo, which were obtained from a 130 ka off-line ice sheet model simulation (Abe-Ouchi et al., 2007).

In LOVECLIM the organic matter that is not remineralized as well as the carbonate and opal that are not dissolved are permanently preserved in the sediments. This leads to a loss of alkalinity, carbon, phosphates and silicates, which is compensated by the river influx of these components (Menviel et al., 2008). For the LOVECLIM equilibrium run, the alkalinity over Dissolved Inorganic Carbon (DIC) ratio in the riverine input was set to 1.6, thus allowing for a greater oceanic carbon reservoir at 50 ka B.P. than at pre-industrial time. In a subsequent 3000 yr equilibrium run atmospheric CO_2 becomes a prognostic variable and the riverine input of alkalinity and DIC then compensates for the loss due to organic matter and carbonate sedimentation. As the UVic ESCM includes a sediment model, no such riverine input adjustment is made and the oceanic carbon reservoir simulated at 50 ka B.P. is smaller than the pre-industrial one. A 3000 yr equilibrium run with prognostic atmospheric CO_2 was also run with the UVic ESCM.

Transient simulations of the period 50–34 ka B.P. (L–Tr and U–Tr) were run with continuously varying orbital and ice sheet forcing following the methodology of Timm et al. (2008), but without any acceleration, and with prognostic atmospheric CO_2. As both models do not include an interactive ice sheet, freshwater withholding from the ocean during phases of ice sheet growth and freshwater release into the ocean as a result of ice sheet calving and ablation are not explicitly captured. To mimic the time-

evolution of these terms and their effect on the oceanic circulation, we apply a freshwater forcing to the North Atlantic region (55°W–10°W, 50°N–65°N) (Fig. 1a). The freshwater forcing time series is obtained through an iterative procedure, that optimizes the anomalous freshwater flux such that the simulated temperature anomalies in the eastern subtropical North Atlantic best match the target alkenone-based SST anomalies reconstructed from the Iberian margin core MD01-2443 (Martrat et al., 2007). Further details on the freshwater forcing applied and the impact on Northern Hemispheric climate in LOVECLIM are discussed in Menviel et al. (2014b). A similar forcing was first applied in both models, but due to the model's sensitivity to freshwater input, the freshwater forcing applied in the UVic ESCM was slightly adjusted.

Moderate changes in the mid/high Southern latitudes hydrological cycle can significantly impact surface salinity. As the atmospheric models used here are simple, it is thus possible that our standard experiments might not capture the past variability of Antarctic Bottom Water accurately. Hence, in subsequent additional transient experiments (L–TrS, U–TrS), a salt flux is added over the Indian and Pacific sides of the Southern Ocean (40°S–50°S, 0°E–120°E; 50°S–62°S, 120°E–280°E, Figs. 2a and 3a). A salt flux (0.1 Sv) is also added over the Eastern Equatorial Pacific (0°N–11°N, 104°W–88°W) in both L–TrS and U–TrS between 39.7 and 38.8 ka B.P. The forcing applied over the Southern Ocean, designed to obtain a better agreement between simulated and estimated Antarctic air temperature anomalies, is equivalent to an increase of evaporation–precipitation of 24 cm/yr (−0.1 Sv) to 48 cm/yr (−0.2 Sv). Over the Southern Ocean at 50 ka B.P., the simulated annual precipitation is 70 cm/yr compared to an annual evaporation of 50 cm/yr. Instead of the Southern Pacific and Indian Ocean being regions of negative evaporation–precipitation, they become neutral or slightly positive.

In addition, while the vegetation cover is allowed to vary, the terrestrial carbon reservoir is decoupled in the experiments described above to isolate and thus better understand the changes in the oceanic carbon reservoir. The effect of terrestrial carbon reservoir changes is tested in additional experiments L–TrV, L–TrVS, U–TrV and U–TrVS, which are similar to respectively L–Tr, L–TrS, U–Tr and U–TrS (Table S1). Experiments L–TrV and L–TrVS are only performed for the period 42–36 ka B.P.

2.2. Idealized experiment with an eddy-permitting ocean–sea–ice model

Experiments are conducted with the GFDL-MOM025 global ocean–sea–ice model, which is based on the Geophysical Fluid Dynamics Laboratory CM2.4 and CM2.5 coupled climate models (Farneti et al., 2010; Delworth et al., 2012). The model has a 1/4° horizontal resolution with a bipolar Arctic north of 65°N and a Mercator grid south to 65°S. The model has 50 vertical levels and is coupled to the GFDL Sea Ice Simulator dynamic/thermodynamic sea–ice model. The atmospheric state for ACCESS-OEP is prescribed and converted to ocean surface fluxes by bulk formulae, consequently the model does not resolve air–sea feedbacks. The atmospheric forcing for all ACCESS-OEP simulations is derived from version 2 of the Coordinated Ocean-ice Reference Experiments Normal Year Forcing (CORE-NYF) reanalysis data (Griffies et al., 2009; Large and Yeager, 2009). CORE-NYF provides a climatological mean atmospheric state at 6-h intervals for 1 yr and includes synoptic variability.

The control ACCESS-OEP simulation (CNTRL) was equilibrated with 100 yr of Normal Year Forcing (CORE-NYF). In CNTRL the sea surface salinity is restored at every ocean grid point to an observed seasonally-varying climatology on a 60-day time-scale over the upper 10 m grid cell. An enhanced AABW water mass transformation experiment (ANT_{SALT}) is initiated from year 100 of CNTRL. In ANT_{SALT} the sea surface salinity restoring climatology is the same as CNTRL, except within 4° latitude of the Antarctic coastline where it is increased by 0.5 psu. The restoring time-scale remains fixed at 60 days. Both ANT_{SALT} and CNTRL are integrated for an additional 40 years. To address linear model drift, anomalies are determined by differencing ANT_{SALT} from the concomitantly extended CNTRL simulation.

3. Simulating the transient climate evolution during MIS3

3.1. Results of standard transient experiments

As discussed in Menviel et al. (2014b), the simulated AMOC changes during MIS3 in LOVECLIM (L–Tr, Fig. 1b) yield a ∼9 °C surface air temperature decrease over Greenland and a 3 °C sea surface cooling off the Iberian margin during Heinrich stadials, in good agreement with paleoproxy records (Fig. 1, blue lines) (Huber et al., 2006; Martrat et al., 2007). The UVic ESCM also simulates changes in North Atlantic SST that are comparable to the Iberian margin record (U–Tr, Fig. 1, red lines). The timing of air temperature variations simulated over Greenland with the UVic ESCM is in good agreement with the NGRIP temperature record, but the amplitude is small due to damping by the large sea ice cover over the Greenland and Norwegian Seas during Interstadials (not shown).

As seen in Fig. 1e, the air temperature over Antarctica increases by only 0.6 °C in experiments L–Tr and U–Tr during AIM12 (49–45 ka B.P.) and AIM8 (40–37 ka B.P.). In contrast, temperature estimates from EPICA Dome C ice core (Jouzel et al., 2007) suggest a 2 °C increase during these events. More importantly, in both models, the amplitude of the simulated warming over Antarctica is similar for all the events, i.e. the amplitude of AIM8 is similar to that of AIM7, whereas the amplitudes of the temperature estimate (Brook et al., 2005; Jouzel et al., 2007; Uemura et al., 2012), sodium flux (Röthlisberger et al., 2002) and atmospheric CO_2 anomalies (Bereiter et al., 2012; Ahn and Brook, 2014) recorded in Antarctic ice cores are much larger for AIM12 and AIM8 than for AIM11, AIM10 and AIM7 (Fig. 1).

In the model experiments, atmospheric CO_2 is prognostic and increases by 10 to 15 ppmv at the end of AIM12 and AIM8 due to the AMOC resumption (Fig. 1g). Experiments performed with both LOVECLIM and the UVic ESCM thus fail to simulate the atmospheric CO_2 increase occurring during AIM12 and AIM8 (Bereiter et al., 2012; Ahn and Brook, 2014).

We perform an additional experiment with LOVECLIM forced with the Antarctic ice core CO_2 evolution as recorded in the EDML ice core (not shown) to evaluate the impact of the atmospheric CO_2 forcing on Antarctic air temperature. Such a simulation does not lead to a different air temperature anomaly evolution over Antarctica during AIM12. During AIM8, instead of showing a very short lived Antarctic positive air temperature anomaly, forcing with the recorded pCO_2 evolution extends the positive air temperature anomaly over Antarctica for the duration of HS4, thus reducing the mismatch. However, the simulation still does not capture the full amplitude of the warming. The climate sensitivity of LOVECLIM in the version used here is 2.04 °C and 3.12 °C respectively for transient and equilibrium simulations. This climate sensitivity is very close to the CMIP5 multi-model mean (1.8 and 3.2 °C respectively; Flato et al., 2013) and thus we doubt that a low climate sensitivity could explain the discrepancy between model and paleoproxy records.

The transient experiments performed by both models clearly show that the initiation of the Antarctic warming is in phase with the AMOC shutdown (Fig. 1). The warming over Antarctica attains its maximum amplitude in both models about 100 yr after the total shutdown of the AMOC. A second peak warming is simulated in both models, at the very beginning of the AMOC recovery and is

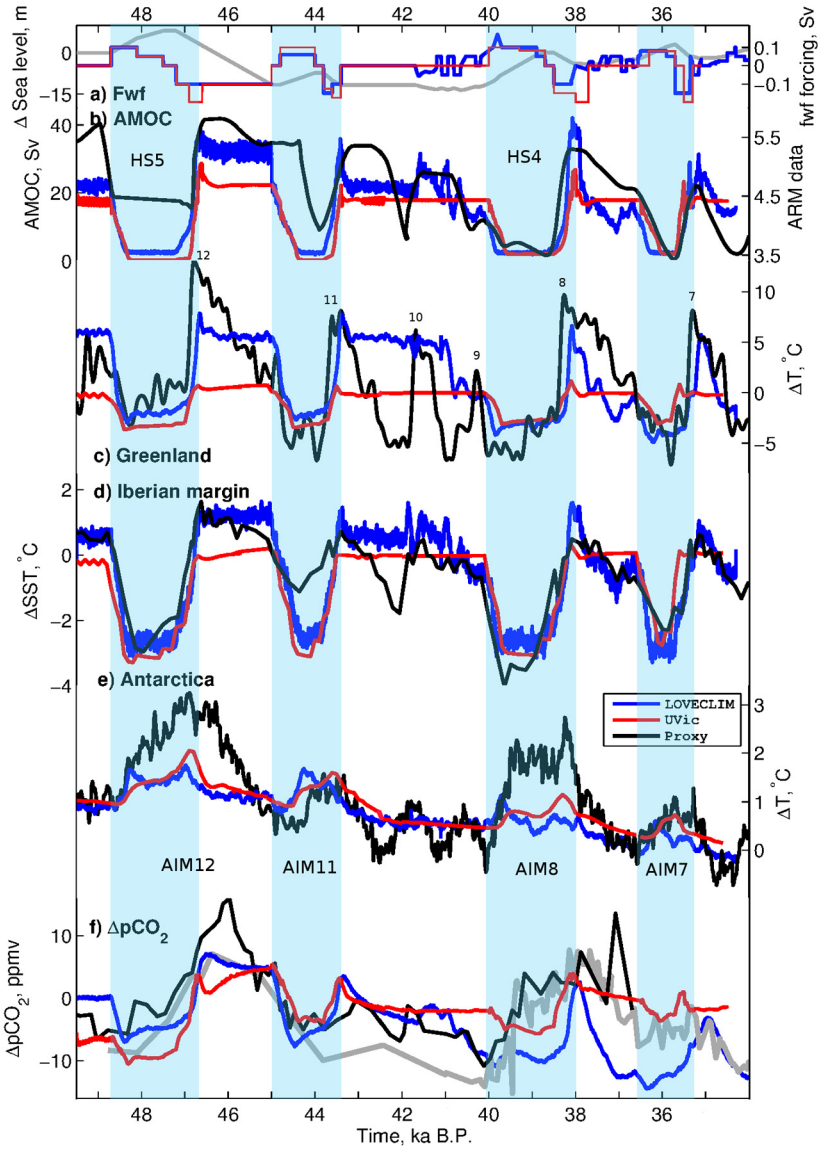

Fig. 1. Timeseries of a) applied North Atlantic (LOVECLIM in blue, the UVic ESCM in red) freshwater forcing (Sv) and associated change in global mean sea level (m, grey); b) simulated maximum meridional overturning circulation in the North Atlantic (Sv) compared to North Atlantic marine sediment cores ARM data (Kissel et al., 2008); c) simulated NE Greenland air temperature anomalies (40°W–10°E, 66°N–85°N) compared to the NGRIP temperature reconstruction (Huber et al., 2006) on the GICC05 timescale (Svensson et al., 2008), with DO numbers; d) simulated SST anomalies off the Iberian margin (15°W–8°W, 37°N–43°N) compared to alkenone-based SST anomalies from marine sediment core MD01-2444 (Martrat et al., 2007) on the GICC05 timescale; e) air temperature anomalies (°C) averaged over Antarctica (90°S–75°S) compared to temperature anomaly estimates from EPICA Dome C ice core (Jouzel et al., 2007) on the EDC3 time-scale (Parrenin et al., 2007), shifted by −400 yr; f) simulated atmospheric CO_2 anomalies (ppmv) compared to pCO_2 anomalies measured in EDML and Talos Dome ice cores (Bereiter et al., 2012) (black) and Siple Dome ice core (Ahn and Brook, 2014) (grey). Paleoproxy records are in grey, experiment L–Tr is in blue and U–Tr in red. The light blue shading indicates the main stadials of MIS3. (For interpretation of the references to color in this figure, the reader is referred to the web version of this article.)

associated with increased atmospheric CO_2 and enhanced Antarctic Bottom Water formation (Figs. 2b, g and 3b, g). After this initial warming, Antarctic temperature decreases in both models. When the AMOC reaches its full amplitude, Antarctic temperature has fully recovered as well.

Meridional heat transport reorganization due to AMOC changes (Crowley, 1992; Stocker, 1998) can explain the moderate Antarctic warming observed during AIM11, AIM10 and AIM7, as well as the initial warming occurring during AIM12. In our simulations performed with LOVECLIM and the UVic ESCM, the poleward heat transport averaged between 20°S and 70°S increases by respectively 15% and 6% during the AMOC shutdown. However, changes in meridional heat transport due to AMOC changes cannot fully explain the largest events AIM12 and AIM8. Here we hypothesize that changes in North Atlantic Deep Water might not be sufficient to explain high Southern latitude climate change and we further suggest that changes in Antarctic Bottom Water could modulate high Southern latitude climate as well as the marine carbon cycle.

3.2. Results of transient experiments with episodic enhancement of Antarctic Bottom Water formation

The standard transient experiments (L–Tr and U–Tr) display 0.7 and 1.4 °C warming respectively over Antarctica and at the surface of the Southern Ocean during all the AIM of Marine Isotope Stage 3 (Figs. 2 and 3, blue lines). While in these experiments AABW displays a slight weakening as the AMOC shuts down, followed by a 3 to 5 Sv increase during the AMOC recovery, experiments forced with an additional salt flux over the Southern Ocean (equivalent to a net E–P anomaly of 24 to 48 cm/yr) simulate ∼10 Sv stronger AABW.

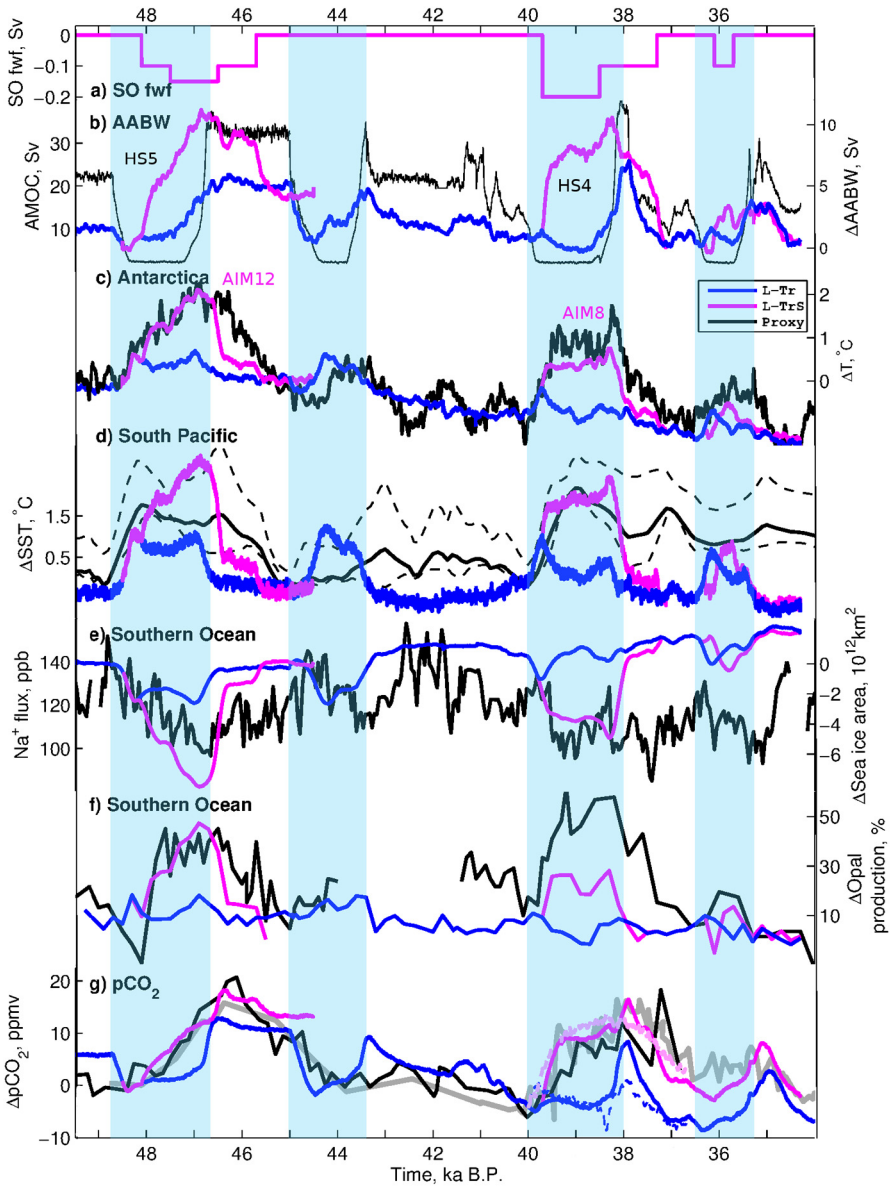

Fig. 2. Transient LOVECLIM simulations (L–Tr, blue and L–TrS, magenta) compared to paleoproxy records (black). Timeseries of a) applied buoyancy forcing (Sv) over the Southern Ocean; b) simulated changes in Antarctic Bottom Water (AABW, Sv) and in the AMOC (Sv, grey); c) air temperature anomalies (°C) averaged over Antarctica (90°S–75°S) compared to temperature anomaly estimates from EPICA Dome C ice core (Jouzel et al., 2007) on the EDC3 time-scale (Parrenin et al., 2007) (black); d) SST anomalies averaged over the South Pacific Ocean (120°E–285°E, 55°S–35°S) compared to a SST anomaly composite from South Pacific marine sediment cores (Pahnke et al., 2003; Kaiser et al., 2005; Caniupán et al., 2011; Lopes dos Santos et al., 2013). Dashed black lines represent the +1 and −1 standard deviation of the composite; e) simulated sea–ice area ($\times 10^{12}$ m^2) over the Southern Ocean compared to the sea salt flux (Na^+) measured in EPICA Dome C ice core (black) (Röthlisberger et al., 2002) on the EDC3 time-scale (Parrenin et al., 2007); f) opal production anomaly (%) averaged over the South Atlantic Ocean (50°W–20°E, 42°S–60°S) compared to the opal flux anomaly (%) record from South Atlantic marine sediment core TNO57-14PC (Anderson et al., 2009); g) simulated atmospheric CO_2 (ppmv) anomalies compared to pCO_2 anomalies measured in EDML and Talos Dome ice cores (Bereiter et al., 2012) (black) and Siple Dome ice core (Ahn and Brook, 2014) (grey). Experiments L–TrV and L–TrVS are in dashed blue and magenta respectively. The South Pacific SST anomaly composite was generated by aligning the individual SST records of marine sediment cores MD97-2120 (Pahnke et al., 2003), ODP 1233 (Kaiser et al., 2005), MD07-3128 (Caniupán et al., 2011) and MD03-2607 (Lopes dos Santos et al., 2013) onto the EDML $\delta^{18}O$ records. For core MD03-2607 the Uk37 SST estimate was used. The EPICA Dome C ice core temperature and nss Ca^{2+} estimates were shifted by −400 yr. Due to the tuning used for the stratigraphy of core TNO57-14PC (Anderson et al., 2009), AIM12 was centered around 45 ka B.P. We thus shifted the 47 to 41 ka B.P. portion of the record by −2600 yr. (For interpretation of the references to color in this figure, the reader is referred to the web version of this article.)

In our experiments, a strengthening of AABW transport has a significant impact on Southern Hemispheric climate but does not lead to any significant changes in Northern Atlantic air or sea surface temperature (not shown). Stronger AABW during AIM12 and AIM8 doubles the simulated warming at high Southern latitude thus leading to 1.5–2 °C temperature increase over Antarctica and at the surface of the Southern Ocean, in better agreement with paleoproxy records (Figs. 2 and 3, magenta lines). Estimates from Antarctic ice core records (Brook et al., 2005; Jouzel et al., 2007; Uemura et al., 2012) as well as SST proxy records (e.g. Pahnke et al., 2003; Crosta et al., 2004; Kaiser et al., 2005; Pahnke and Zahn, 2005; Caniupán et al., 2011; Lopes dos Santos et al., 2013) suggest a 2 to 3 °C warming over Antarctica and the Southern Ocean, respectively, during AIM12 and AIM8. While quantitative estimates of these warming events are subject to uncertainties, the anomalies registered for AIM12 and AIM8 are much larger than for the other Antarctic Isotope Maxima (i.e. AIM11, 10, 9 and 7). In addition, Southern Hemispheric sea–ice area is now reduced by about 40% in experiments L–TrS and U–TrS compared to 10% in experiments L–Tr and U–Tr (Figs. 2 and 3).

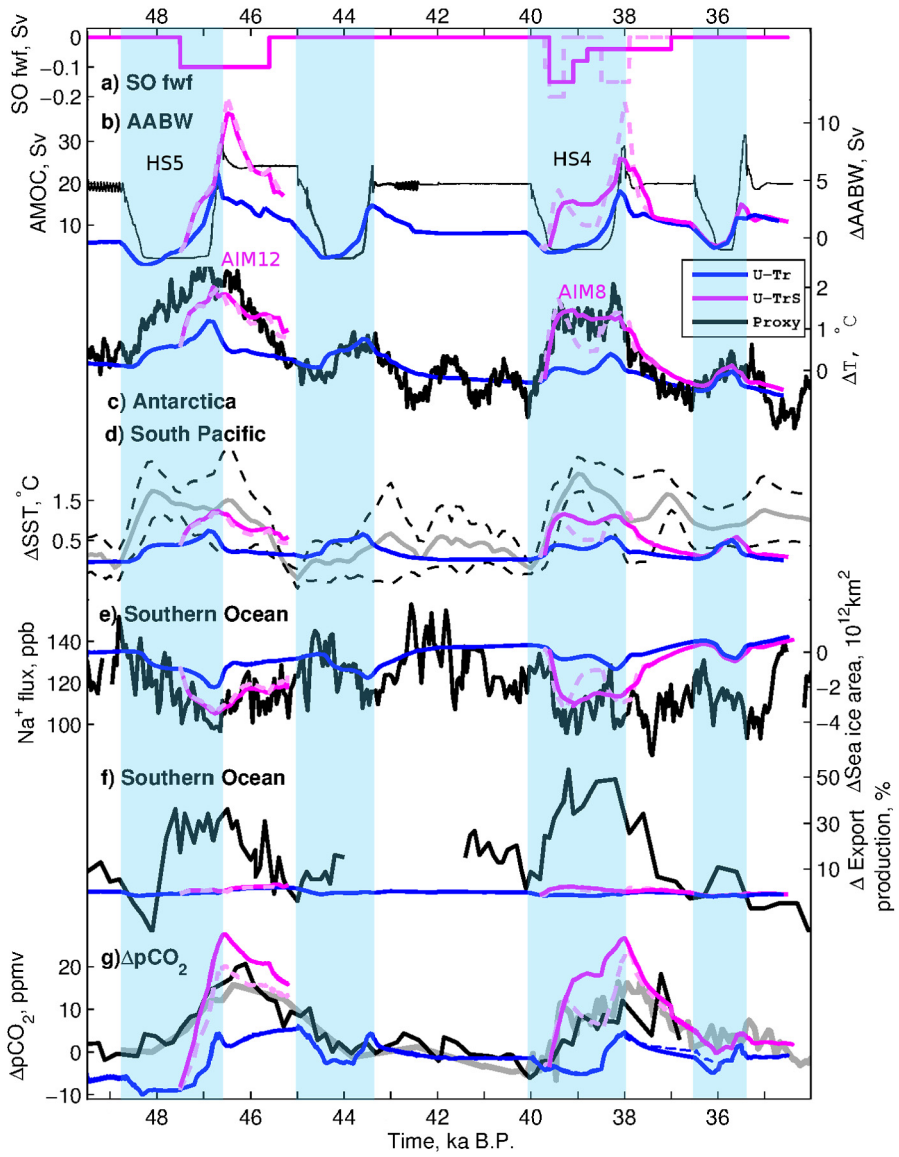

Fig. 3. Same as Fig. 2, but for experiments performed with the UVic ESCM: U–Tr (solid blue), U–TrS (solid magenta), U–TrV (dashed blue) and U–TrVS (dashed pink). (For interpretation of the references to color in this figure, the reader is referred to the web version of this article.)

Enhanced AABW formation in LOVECLIM and the UVic ESCM leads to stronger downwelling and convective overturn south of 70°S and stronger upwelling between 60°S and 70°S. As Circumpolar Deep Water is slightly warmer than the overlying surface waters, enhanced convection over the Southern Ocean leads to warmer conditions at the surface, while inducing a ∼0.4 °C subsurface cooling south of 60°S as well as below 2000 m (Fig. 4). In LOVECLIM, the oceanic poleward heat transport averaged between 20°S and 70°S increases by an additional 12% when the AABW is enhanced by 10 Sv, thus explaining the additional Southern Ocean warming. As the AMOC shuts down, the Antarctic Circumpolar Current (ACC) strengthens by 10% and enhanced AABW formation further strengthens the ACC by another 12% (not shown). The ACC is not only zonal but has a meridional component at certain longitudes, and thus plays a role in transporting heat poleward (Volkov et al., 2010).

The modes of variability associated with changes in North Atlantic Deep Water (NADW) and AABW are highlighted in an Empirical Orthogonal Function (EOF) analysis performed on experiments L–TrS and U–TrS (Fig. 5). As seen by the high correlation between the time evolution of the first EOF and normalized air temperature anomalies inferred from NGRIP, Greenland (Fig. 5 left), the first EOF of the simulated air temperature is associated with changes in NADW and only shows a ∼0.5 °C warming over Antarctica following an AMOC shutdown. Stronger AABW (2nd EOF) enhances the high southern latitude warming, in phase with the AIM, particularly in the latitudinal band 60–80°S (Fig. 5 right). The results of this EOF analysis are in agreement with a regression of the simulated air temperature on changes in NADW and AABW, respectively (not shown), which support the fact that the 1st EOF is associated with changes in NADW and the 2nd with AABW variations.

In LOVECLIM the high southern latitude warming comes to an abrupt end during the AMOC recovery. The poleward heat transport between 20°S and 70°S increases by ∼15% when the AMOC shuts down and can increase a further 12% when the AABW is enhanced, thus reaching ∼27% greater poleward heat transport to high southern latitudes. However, as the AMOC recovers the poleward heat transport anomaly ends. Enhanced AABW can delay the Antarctic cooling by about 200 yr following the AMOC resumption.

On the other hand, in the UVic ESCM, stronger AABW still leads to positive temperature anomalies over high southern latitudes

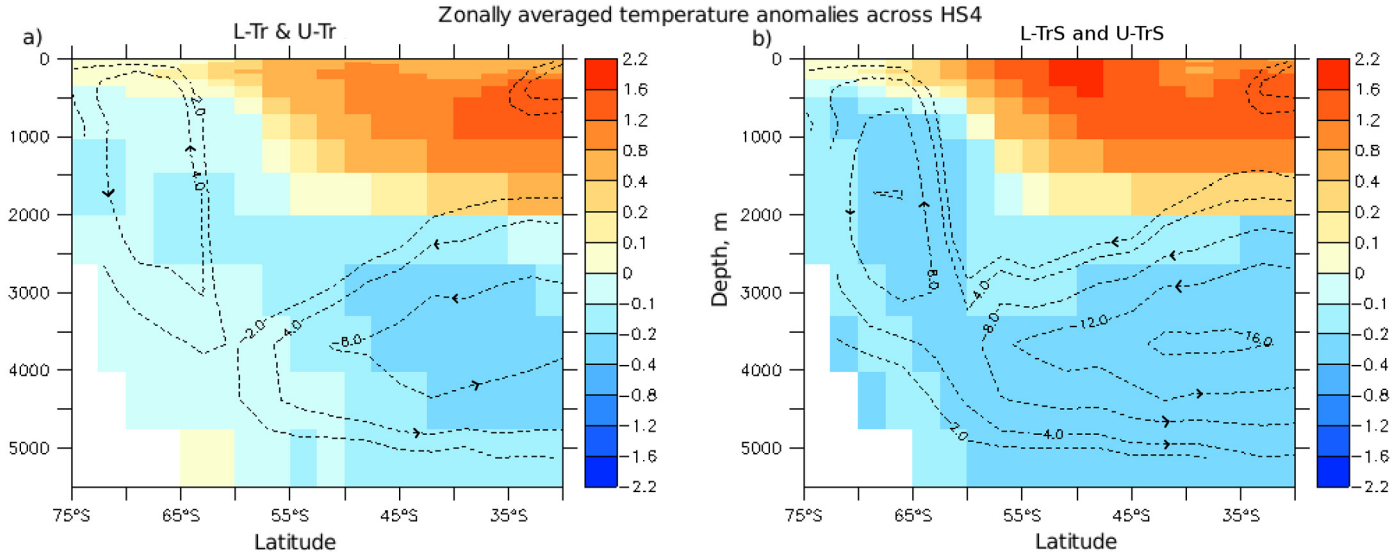

Fig. 4. Composite of zonally averaged ocean temperature anomalies (°C) across HS4 (AIM8) (10 yr averaged of 39.2 ka B.P. compared to 10 yr averaged of 41.7 ka B.P.) for (a) experiments L–Tr and U–Tr and (b) experiments L–TrS and U–TrS. Overlaid is a composite of the globally averaged streamfunction for a 10 yr average at 39.2 ka B.P. Only negative values of the globally averaged streamfunction are shown and the circulation is counter-clockwise.

during and after the AMOC recovery. This is first explained by the weak effect of AMOC changes on high southern latitudes temperature in the UVic ESCM. It could also be due to the higher Gent and McWilliams thickness diffusion coefficient in the UVic ESCM (800 m^2/s) compared to LOVECLIM (200 m^2/s).

As a summary, without any changes in AABW, there is no lag between the Antarctic cooling and the AMOC recovery, and the full amplitude of the large Antarctic Isotope Maxima (AIM12 and AIM8) cannot be simulated. If changes in poleward heat transport drive the high southern latitude warming and the AABW formation is enhanced, as is the case in LOVECLIM, then the Antarctic cooling will lag the AMOC recovery by a maximum of 200 yr. This indicates that high southern latitude climate is more sensitive to an AABW strengthening when the AMOC is weak than when it is strong. As the AMOC strengthens, heat is transported to the North Atlantic and the high southern latitudes cool, overwhelming the surface air temperature warming due to AABW variations.

4. Simulating the transient evolution of atmospheric CO_2

In Section 3.2 we have shown that changes in AABW could play a significant role in modulating Southern Hemisphere climate during a shutdown of the AMOC, with stronger AABW leading to warmer conditions at high southern latitudes. In this section we show that strong AABW formation during the AMOC cessation could lead to an atmospheric CO_2 increase.

In the standard transient experiments performed with LOVECLIM and the UVic ESCM, atmospheric CO_2 shows little change or decreases by a few ppmv as the AMOC shuts down (Figs. 2 and 3, blue lines). But, as the deep Atlantic ventilation resumes, atmospheric CO_2 increases by ~10 ppmv. The larger and the longer the AMOC shutdown, the larger the atmospheric CO_2 increase during the resumption. Increased solubility due to colder and fresher conditions during stadials, primarily in the North Atlantic basin, enhances the carbon storage in the deep Atlantic (Menviel et al., 2014a) (Figs. 6a, S5 and S6). The Atlantic carbon reservoir increase can be further explained by the longer residence time in that basin, which leads to an increase in remineralized nutrients (Figs. S2 and S3).

However, high resolution ice core records from Antarctica suggest that atmospheric CO_2 started to increase at ~47.8 ka B.P. during AIM12 and ~39.8 ka B.P. during AIM8 (Ahn and Brook, 2008, 2014; Bereiter et al., 2012), thus during times of weak AMOC. While the standard experiments simulate little atmospheric CO_2 change during that time, experiments in which the AABW strengthens display an atmospheric CO_2 increase of ~13 ppmv (Figs. 2g and 3g). The ventilation of deep and bottom Pacific water in experiments with enhanced AABW and NPDW (L–TrS and U–TrS) releases deep Pacific carbon through the Southern Ocean (Fig. 6b, see also Menviel et al., 2014a).

High-resolution records from the Southern Ocean suggest that the opal flux and marine export production increased significantly during AIM12 and AIM8 (Sachs and Anderson, 2005; Anderson et al., 2009). Our standard transient experiments display no significant changes (L–Tr) or slightly reduced (U–Tr) export production in the Southern Ocean during these events in contrast with the proxies (Fig. S1). However, enhanced AABW in experiment L–TrS increases the upwelling of nutrient rich waters. Stronger AABW production also leads to a poleward shift of the sea–ice edge and a warming of the surface waters. The combination of these changes lead to a 20 to 40% increase in opal and marine export production over the Southern Ocean (Fig. 2f, Fig. S1) in LOVECLIM.

If we decompose the DIC response into contributions from the soft-tissue pump (ΔC_{soft}) and the carbonate pump (see Supplementary Material) (Kwon et al., 2009, 2011), then most of the DIC changes can be explained by ΔC_{soft} in all experiments performed here (Figs. S2 and S3). As NADW slows down, the deep Atlantic ventilation decreases and respired carbon accumulates. ΔC_{soft} thus increases in the Atlantic Ocean in both models. In contrast, as AABW and NPDW strengthen, less respired carbon accumulates and more carbon is transferred from depth to the surface (Figs. 6b).

Figs. S2 and S3 show that ΔC_{soft} decreases above 3000 m in the Pacific Ocean in both models as well as in the Southern Ocean in experiment U–TrS. In LOVECLIM, export production increases over the Southern Ocean when AABW strengthens (Fig. S1), which would tend to decrease atmospheric CO_2 and thus provide a negative feedback. This enhanced export production over the Southern Ocean reduces the preformed nutrient content exported in AABW (Marinov et al., 2006) and could explain the lack of ΔC_{soft} change in the Southern Ocean in experiment L–TrS, compared to experiment U–TrS.

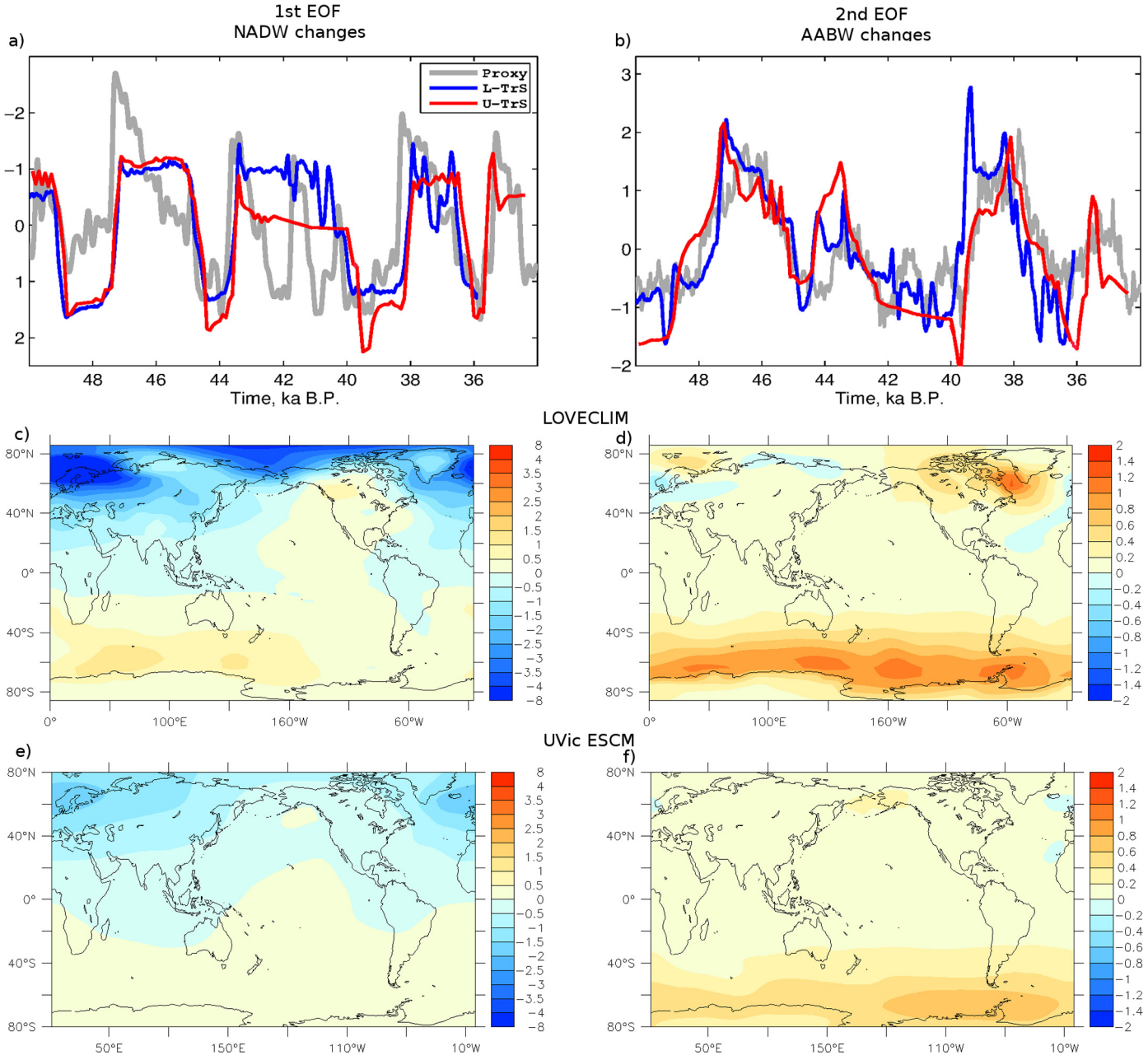

Fig. 5. First (left) and second (right) EOF of detrended air temperature anomalies. (a, b) Normalized principal component of EOF of detrended air temperature anomalies for experiments L–TrS (blue) and U–TrS (red) compared to normalized Greenland NGRIP (e) (Huber et al., 2006) and Antarctic (f) (Parrenin et al., 2007) ice core temperature anomaly records (grey). EOF pattern for (c, d) experiment L–TrS and (e, f) experiment U–TrS; The 1st (2nd) EOF explains 88% (8%) and 76% (21%) of the variance for LOVECLIM and the UVic ESCM respectively. (For interpretation of the references to color in this figure legend, the reader is referred to the web version of this article.)

A small contribution of ΔC_{carb} (~20%) is found in the deep North Atlantic for experiments performed with LOVECLIM. Reduced ventilation in the deep North Atlantic leads to a DIC increase, which increases the corrosiveness of the water, increases carbonate dissolution and thus leads to a small alkalinity increase (Fig. 6c). This decrease in deep South Atlantic ocean carbonate ion content (not shown) is in agreement with paleoproxy reconstructions (Yu et al., 2014). Changes in ΔC_{carb} are also significant at intermediate depth in the North Pacific, whereby enhanced NPDW reduces the vertical alkalinity gradient by bringing high alkalinity waters to the surface. It should be noted that ΔC_{carb} contributions to changes in pCO_2 are an order of magnitude smaller than the ΔC_{soft} contributions (Fig. S4).

In experiments where the terrestrial carbon reservoir is kept constant, changes in atmospheric CO_2 are mostly due to changes in the partial pressure of CO_2 at the ocean's surface, which is in turn a function of changes in temperature, salinity, DIC and Alkalinity (see Supplementary Material). Solubility changes can explain up to 50% of the pCO_2 variations in experiments L–Tr, L–TrS and U–Tr (Figs. S5a and S6a). Stronger NPDW and AABW also induce relatively warm and saline conditions at the surface of the Pacific Ocean, thus decreasing CO_2 solubility and leading to an atmospheric CO_2 increase (Menviel et al., 2014a) (Figs. S4a and S5a).

As the mean surface ocean alkalinity (ALK) and DIC are the same order of magnitude and the Revelle factors of DIC and alkalinity are 10 and −9.4 respectively (Takahashi et al., 1993), changes in surface ocean pCO_2 due to alkalinity and DIC are a function of $\Delta DIC - \Delta ALK$ (Sarmiento and Gruber, 2006) (see Supplementary Material). Similar to DIC, alkalinity is much higher in the deep ocean than at the surface, particularly in the Pacific

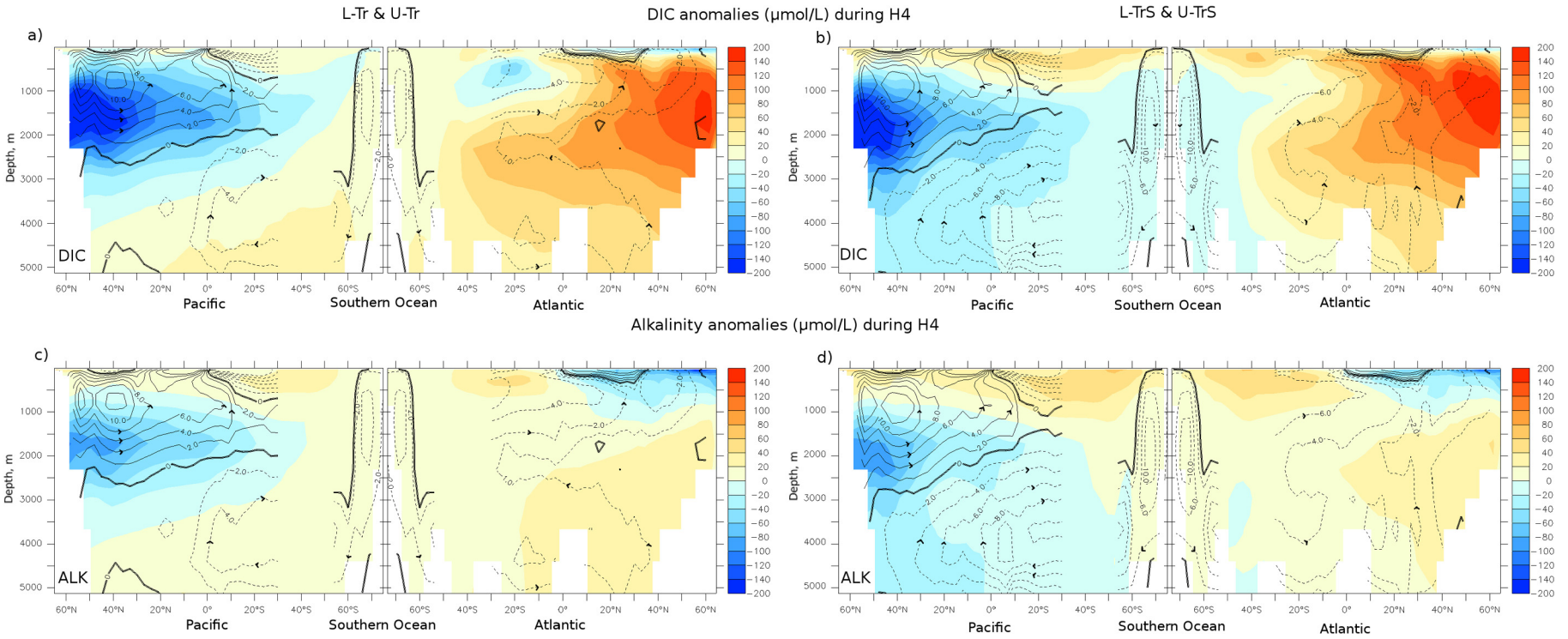

Fig. 6. DIC (top) and alkalinity (bottom) anomalies (μmol/L) during HS4 (39.1 ka B.P.) compared to 40 ka B.P. for (left) a composite of standard experiments (L–Tr and U–Tr) and (right) a composite of experiments with enhanced AABW (L–TrS and U–TrS). Overlaid are composite of respectively the Pacific, global (for the Southern Ocean) and Atlantic streamfunction for a 10 yr average at 39.1 ka B.P. The sense of flow is indicated by the arrows.

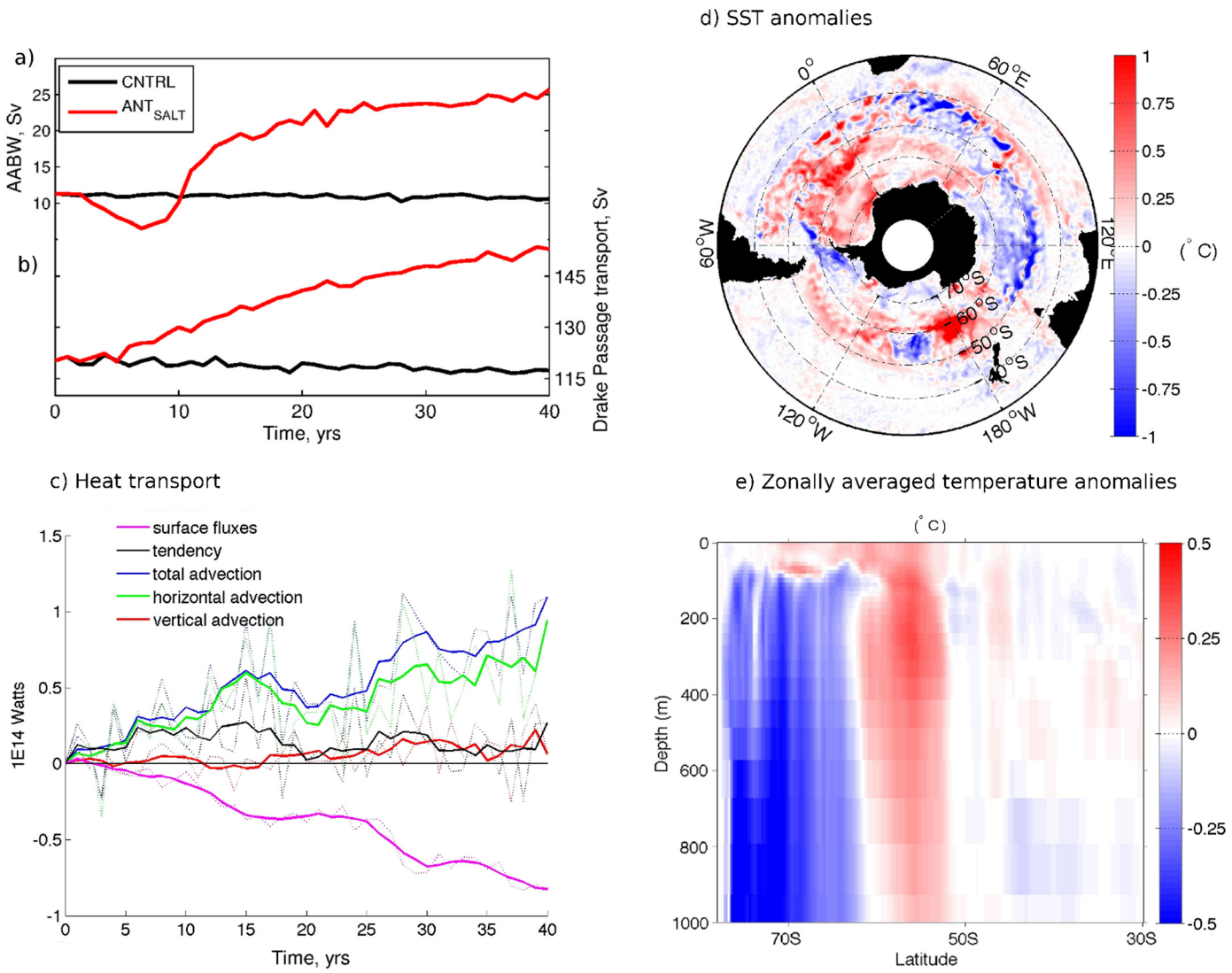

Fig. 7. Results of the experiment performed with a global eddy-permitting ocean sea–ice model: Timeseries of a) maximum transport in the lower cell (Sv) and b) transport across the Drake Passage (Sv) for experiments CNTRL (black) and ANT_{SALT} (red); c) Timeseries of non-negligible annual mean heat tendency anomaly (10^{14} Watts) integrated between 50–60°S and over the upper 1000 m of the ocean in experiment ANT_{SALT}, showing that the Southern Ocean SST increase is mainly due to greater horizontal heat advection (green line) with a significant SAT damping (magenta). Solid lines represent a 5-yr running mean. See Appendix A for details on the heat budget calculations. d) Annual mean SST anomalies (°C) and e) zonally averaged ocean temperature anomalies (°C) for ANT_{SALT} compared to CNTRL and averaged over years 31–40.

(Key et al., 2004). Enhanced ventilation of the deep Pacific thus also induces an alkalinity increase at the surface of the Pacific and Southern Oceans (Figs. 6d, S4b and S5b), which dampens the surface ocean pCO_2 increase. During an AMOC shutdown, the sensitivity of enhanced AABW to atmospheric CO_2 increase will thus depend on the initial vertical gradient of DIC–ALK. As this vertical gradient is higher in the 50 ka control run of the UVic ESCM than in the LOVECLIM 50 ka control run, the UVic ESCM displays a higher sensitivity to changes in AABW (Figs. S5b and S6b). The lower sensitivity of the atmospheric CO_2 response to changes in AABW in LOVECLIM could also be explained by the enhanced nutrient drawdown over the Southern Ocean in that model.

5. Impact of enhanced Antarctic Bottom Water formation on SST: experiments with an eddy-permitting ocean–sea–ice model

In Section 3.2 we have shown that enhanced AABW formation leads to a high southern latitude warming in two Earth System model through stronger meridional heat transport towards the high Southern latitudes. However, in coarse resolution models, such as the version of LOVECLIM and the UVic ESCM used here, a number of important oceanic heat transport processes are not adequately represented. For example, the width of ocean currents is over-estimated, while their speeds are underestimated, and the influence of mesoscale eddies are parameterized with a fixed Gent–McWilliams diffusion parameter (Bryan et al., 2014). In order to test whether a warming of the Southern Ocean due to enhanced AABW formation is a robust feature, we perform further experiments using a global mesoscale eddy-permitting ocean-sea–ice model (GFDL-MOM025).

Increasing the surface salinity close to the Antarctic coast in the high-resolution experiment ANT_{SALT} deepens the mixed layer by up to 400 m in parts of the Weddell and Ross Seas, leading to an increase in AABW formation from 12 to 25 Sv (Fig. 7a). The saltier water near Antarctica enhances the meridional density gradient across the Southern Ocean, inducing a 28% increase in the Antarctic Circumpolar Current (ACC) transport through Drake Passage (Fig. 7b). The poleward heat transport between 20°S and 70°S increases by 29%, which is twice the increase obtained in the coarse resolution models. As expected, the SST response is more spatially variable than found at coarse resolution (Fig. 7d); it increases by up to 1 °C between 50°S and 70°S in the Pacific sector and be-

tween 45°S–75°S in the Atlantic sector and decreases by up to 1 °C in the Indian sector of the Southern Ocean (40°S–50°S, 20°E–70°E and 50°S–60°S, 80°E–140°E). The zonal average SST increases by 0.1 °C between 50°S–70°S, and the upper 1000 m ocean temperature between 50°S–60°S increases by 0.15 °C (Fig. 7e). It should be noted, however, that the 10 m atmospheric fields felt by the GFDL-MOM025 ocean–sea ice model are fixed to a prescribed climatology. In particular, the Surface Air Temperature (SAT) boundary condition highly constrains the SST response to perturbations, unlike in a fully coupled model where SST anomalies can grow in amplitude due to coupled air–sea feedbacks. If the SAT constraint was removed, one may expect even greater SST warming over the Southern Ocean in response to AABW invigoration.

The physical processes impacting the upper 1000 m ocean heat content between 50°S–60°S were determined via online heat budget calculations in GFDL-MOM025 (see Appendix A). The ocean heat budget decomposition shows that the warming is primarily caused by horizontal advection tendencies explicitly resolved by the model (Fig. 7c). Heating tendencies associated with changes in near surface processes (e.g. surface buoyancy fluxes) have an overall cooling effect, and changes due to vertical advection and parameterized mixing processes are small. As shown in previous studies, the horizontal advection heating tendencies are associated with both resolved mesoscale processes and large-scale zonal asymmetries in ACC transport (Volkov et al., 2010; Spence et al., 2012).

6. Discussion and conclusions

We have shown that AMOC changes can explain the small amplitude Antarctic Isotope Maxima (e.g. AIM10, AIM9 and AIM7), but cannot fully explain the amplitude of the large events (i.e. AIM12 and AIM8) nor the long duration of AIM12.

The meridional heat transport reorganization due to AMOC changes leads to 0.5–1 °C temperature increase over Antarctica and at the surface of the Southern Ocean (Kageyama et al., 2013). In contrast, paleoproxy records suggest a 2 °C warming over Antarctica and at the surface of the Southern Ocean during AIM12 and AIM8 (Pahnke et al., 2003; Crosta et al., 2004; Kaiser et al., 2005; Jouzel et al., 2007; Parrenin et al., 2007; Caniupán et al., 2011; Lopes dos Santos et al., 2013). Paleoproxy records also suggest a strong decrease in Southern Hemispheric sea–ice area (Röthlisberger et al., 2002) and enhanced Southern Ocean opal production (Anderson et al., 2009) during AIM12 and AIM8. While significant uncertainties are associated with the quantitative reconstructions of these events, AIM12 and AIM8 are much larger in amplitude than the other Antarctic Isotope Maxima of Marine Isotope Stage 3 (i.e. AIM 11, 10, 9 and 7) in all high southern latitude proxy records. The amplitude of these events cannot be captured by our transient experiments performed with LOVECLIM and the UVic ESCM (L–Tr and U–Tr): we have shown that changes in North Atlantic Deep Water are insufficient to explain high southern latitude records, and that Southern Ocean processes might also play a role in shaping these events.

Our simulations show that without changes in AABW, high southern latitude warming/cooling occurs in phase with the AMOC shutdown/recovery. However, as Broecker (1998) hypothesized, we find that changes in AABW formation modulate Southern Hemispheric climate during a shutdown of the AMOC. Enhanced AABW leads to a greater meridional heat transport to high southern latitudes, a stronger Antarctic Circumpolar Current and greater vertical mixing in the Southern Ocean. A ∼10 Sv stronger AABW leads to ∼2 °C increase in air temperature over Antarctica in the two Earth System models (LOVECLIM and the UVic ESCM) examined here. Enhanced AABW also warms Southern Ocean surface waters by ∼2 °C and ∼1.2 °C in LOVECLIM and the UVic ESCM respectively. This result is confirmed by experiments performed with a global eddy-permitting ocean–sea–ice model, which displays up to 1 °C increase in Southern Ocean surface waters as a result of a ∼10 Sv AABW strengthening, despite the damping effect of a fixed climatological SAT forcing in that model run. Southern Hemispheric sea–ice retreat is further enhanced in simulations displaying stronger AABW. It should be noted that enhanced AABW can also be simulated during an AMOC shutdown if global salt compensation is applied.

Finally, in agreement with ice core records, we find that Greenland stadials have a small impact on atmospheric CO_2. Without any changes in AABW, significant atmospheric CO_2 increases are primarily linked with the resumption of the AMOC at the end of the large Heinrich stadials. Given the GICC05 chronology (Svensson et al., 2008), we suggest that the atmospheric CO_2 increases occurring during Heinrich stadials 5 (∼48–47 ka B.P.) and 4 (∼39.8 ka B.P.) (Ahn and Brook, 2008; Ahn and Brook, 2014) could be explained by enhanced AABW transport (Menviel et al., 2014a). Changes in AABW formation could thus play a significant role in controlling the marine carbon cycle and thus the amount of CO_2 outgassed in the atmosphere during Heinrich stadials.

Enhanced AABW formation during Heinrich stadials could be due to changes in surface buoyancy forcing over the Southern Ocean, not captured in our simulations due to experimental design or due to the simple atmospheric models used. For example, a recent study performed with an iceberg/sediment model (Roberts et al., 2014) suggests that 0.04 Sv of freshwater was released during 500 yr into the North Atlantic during a typical Heinrich event. This is less than half of the freshwater added in our experiments. Spreading of anomalously low salinity waters from the North Atlantic to the Southern Ocean could weaken AABW formation in our experiments. Furthermore, moisture transport from the Atlantic to the Pacific across Central America decreased during Heinrich stadials (Richter and Xie, 2010) and the East Asian summer monsoon weakened (e.g. Wang et al., 2001). These processes, best represented in multi-level high resolution atmospheric GCMs, would contribute to increased surface salinity in the Pacific Ocean, with consequences for Pacific deep and bottom water formation.

AABW formation could also be enhanced during Heinrich stadials due to stronger or poleward shifted Southern Hemisphere Westerlies (Spence et al., 2013; Sheen et al., 2014). For example, Lee et al. (2011) suggested that an AMOC shutdown could induce a 25% increase in the Southern Hemisphere Westerlies via a southward shift of the ITCZ and the correspondent weakening of the Southern Hemisphere Hadley cell. LOVECLIM simulates a 10% weakening of the Southern Hemisphere Westerlies during an AMOC shutdown (Menviel et al., 2008), while there are no significant wind changes in the UVic ESCM due to the negligible wind feedback that operates in that model. The amplitude of the Northern Hemispheric stadial, the origin and timing of the meltwater pulse/iceberg discharge as well as the background climatic conditions might further modulate the AABW response.

Acknowledgements

This project was supported by the Australian Research Council. Model experiments were performed on a computational cluster owned by the Faculty of Science of the University of New South Wales, Australia, as well as on a cluster from the NCI National Facility systems at the Australian National University through the National Computational Merit Allocation Scheme supported by the Australian Government. M. England acknowledges funding from the ARC Laureate Fellowship program (FL100100214). The authors would like to thank Agus Santoso for his advise on statistics as well as two anonymous reviewers and the Editor, Jean Lynch-Stieglitz, for their constructive comments. The authors wish to acknowledge

use of the Ferret program for analysis and graphics in this paper. Ferret is a product of NOAA's Pacific Marine Environmental Laboratory. (Information is available at http://ferret.pmel.noaa.gov/Ferret/.)

Appendix A

Finite volume ocean heat budget.

The physical processes impacting the heat content in each ocean grid volume were calculated online in GFDL-MOM025. The terms required to balance a finite volume heat budget in the ocean model in the upper 1000 m follow Griffies (2012):

$T_{tendency}$ is the net change in the temperature content (i.e., heat) in a grid cell.

$T_{advection}$ is the convergence of the three dimensional advective heat flux components. Additionally, we have separated the $T_{advection}$ term into horizontal and vertical components.

$T_{submeso}$ is the convergence of the three dimensional subgrid-scale flux components arising from the mixed-layer sub-mesoscale parameterization scheme. This term is only non-zero in the mixed layer and so is generally quite small compared to other terms in our domain of interest.

$T_{vert\text{-}diff}$ contains the impacts from vertical diffusion, including regions of gravitational instability, which is handled implicitly in time.

T_{KPP} accounts for the non-local tendency arising from the K-profile parameterization boundary layer scheme. It acts as a redistribution of surface heat fluxes throughout the surface boundary layer. It is quite small in our domain of interest compared to other terms.

$T_{surface\text{-}fluxes}$ accounts for the heat tendency within the upper 50 m associated with surface radiative and buoyancy fluxes, as well as parameterized smoothing of the oceans free surface. It is calculated as the residual difference between $T_{tendency}$ and the summation of the other four terms above.

In summary, $T_{tendency} = T_{advection} + T_{submeso} + T_{vert\text{-}diff} + T_{KPP} + T_{surface\text{-}fluxes}$.

Appendix B. Supplementary material

Supplementary material related to this article can be found online at http://dx.doi.org/10.1016/j.epsl.2014.12.050.

References

Abe-Ouchi, A., Segawa, T., Saito, F., 2007. Climatic conditions for modelling the Northern Hemisphere ice sheets throughout the Ice Age cycle. Clim. Past 3, 423–438.

Ahn, J., Brook, E., 2008. Atmospheric CO_2 and climate on Millennial Time Scales During the Last Glacial Period. Science 322. http://dx.doi.org/10.1126/science.1160832.

Ahn, J., Brook, E., 2014. Siple Dome ice reveals two modes of millennial CO_2 change during the last ice age. Nat. Commun. 5. http://dx.doi.org/10.1038/ncomms4723.

Alley, R., 2000. Ice-core evidence of abrupt climate changes. Proc. Natl. Acad. Sci. USA 97, 1331–1334.

Anderson, R.F., Ali, S., Bradtmiller, L., Nielsen, S., Fleisher, M., Anderson, B., Burckle, L., 2009. Wind-driven upwelling in the Southern Ocean and the deglacial rise in atmospheric CO_2. Science 323, 1443–1448.

Archer, D., 1996. An atlas of the distribution of calcium carbonate in sediments of the deep sea. Glob. Biogeochem. Cycles 10, 159–174.

Bard, E., 2002. Abrupt climate changes over millennial time scales: climate shock. Phys. Today 55, 32–38.

Bereiter, B., Lüthi, D., Siegrist, M., Schüpbach, S., Stocker, T., Fischer, H., 2012. Mode of change of millennial CO_2 variability during the last glacial cycle associated with a bipolar marine carbon seesaw. Proc. Natl. Acad. Sci. USA. http://dx.doi.org/10.1073/pnas.1204069109.

Bouttes, N., Roche, D., Paillard, D., 2012. Systematic study of the impact of fresh water fluxes on the glacial carbon cycle. Clim. Past 8, 589–607.

Bozbiyik, A., Steinacher, M., Joos, F., Stocker, T.F., Menviel, L., 2011. Fingerprints of changes in the terrestrial carbon cycle in response to large reorganizations in ocean circulation. Clim. Past 7, 319–338.

Broecker, W., 1998. Paleocean circulation during the last deglaciation: a bipolar seesaw? Paleoceanography 13, 119–121.

Brook, E.J., White, J., Schilla, A., Bender, M., Barnett, B., Severinghaus, J., Taylor, K., Alley, R., Steig, E., 2005. Timing of millennial-scale climate change at Siple Dome, West Antarctica, during the last glacial period. Quat. Sci. Rev. 24, 1333–1343.

Brovkin, V., Ganopolski, A., Svirezhev, Y., 1997. A continuous climate-vegetation classification for use in climate-biosphere studies. Ecol. Model. 101, 251–261.

Bryan, F., Gent, P., Tomas, R., 2014. Can Southern Ocean eddy effects be parameterized in climate models? J. Climate 27, 411–425.

Buiron, D., Stenni, B., Chappellaz, J., Landais, A., Baumgartner, M., Bonazza, M., Capron, E., Frezzotti, M., Kageyama, M., Lemieux-Dudon, B., Masson-Delmotte, V., Parrenin, F., Schilt, A., Selmo, E., Severi, M., Swingedouw, D., Udisti, R., 2012. Regional imprints of millennial variability during the MIS 3 period around Antarctica. Quat. Sci. Rev. 48, 99–112.

Caniupán, M., Lamy, F., Lange, C., Kaiser, J., Arz, H., Kilian, R., Urrea, O.B., Aracena, C., Hebbeln, D., Kissel, C., Laj, C., Mollenhauer, G., Tiedemann, R., 2011. Millennial-scale sea surface temperature and Patagonian Ice Sheet changes off southernmost Chile (53°S) over the past 60 kyr. Paleoceanography 26. http://dx.doi.org/10.1029/2010PA002049.

Crosta, X., Sturm, A., Armand, L., Pichon, J., 2004. Late Quaternary sea ice history in the Indian sector of the Southern Ocean as recorded by diatom assemblages. Mar. Micropaleontol. 50, 209–223.

Crowley, T., 1992. North Atlantic Deep Water cools the Southern Hemisphere. Paleoceanography 7, 489–497.

Dansgaard, W., Johnsen, S., Clausen, H., 1993. Evidence for general instability of past climate from a 250-kyr ice–core record. Nature 364, 218–220.

Delworth, T., Rosati, A., Anderson, W., Adcroft, A., Balaji, V., Benson, R., Dixon, K., Griffies, S., Lee, H.-C., Pacanowski, R., Vecchi, G., Wittenberg, A., Zeng, F., Zhang, R., 2012. Simulated climate and climate change in the GFDL CM2.5 high-resolution coupled climate model. J. Climate 25, 2755–2781.

Dokken, T., Nisancioglu, K., Li, C., Battisti, D., Kissel, C., 2013. Dansgaard–Oeschger cycles: interactions between ocean and sea ice intrinsic to the Nordic seas. Paleoceanography 28, 491–502.

Eby, M., Montenegro, A., Archer, D., Meissner, K., Weaver, A., 2009. Lifetime of anthropogenic climate change: millennial time scales of potential CO_2 and surface temperature perturbations. J. Climate 22, 2501–2511.

Elliot, M., Labeyrie, L., Bond, G., Cortijo, E., Turon, J.-L., Tisnerat, N., Duplessy, J.-C., 1998. Millennial-scale iceberg discharges in the Irminger Basin during the last glacial period: relationship with the Heinrich events and the environmental settings. Paleoceanography 13, 433–446.

Elliot, M., Labeyrie, L., Duplessy, J.-C., 2002. Changes in North Atlantic deep-water formation associated with the Dansgaard–Oeschger temperature oscillations (60–10 ka). Quat. Sci. Rev. 21, 1153–1165.

EPICA, community members, 2006. One-to-one coupling of glacial climate variability in Greenland and Antarctica. Nature 444, 195–198.

Farneti, R., Delworth, T., Rosati, A., Griffies, S., Zeng, F., 2010. The role of mesoscale eddies in the rectification of the Southern Ocean response to climate change. J. Phys. Oceanogr. 40, 1539–1557.

Flato, G., Marotzke, J., Abiodun, B., Braconnot, P., Chou, S.-C., Collins, W., Cox, P., Driouech, F., Emori, S., Eyring, V., Forest, C., Gleckler, P., Guilyardi, E., Jakob, C., Kattsov, V., Reason, C., Rummukainen, M., 2013. Evaluation of climate models. In: Climate Change 2013: The Physical Science Basis. Contribution of Working Group I to the Fifth Assessment Report of the Intergovernmental Panel on Climate Change. Cambridge Univ. Press, Cambridge, United Kingdom and New York, NY, USA, pp. 741–858.

Fleitmann, D., Cheng, H., Badertscher, S., Edwards, R., Mudelsee, M., Göktürk, O., Fankhauser, A., Pickering, R., Raible, C., Matter, A., Kramers, J., Tüysüz, O., 2009. Timing and climatic impact of Greenland interstadials recorded in stalagmites from northern Turkey. Geophys. Res. Lett. 36, L19707.

Goosse, H., Brovkin, V., Fichefet, T., Jongma, J., Huybrechts, P., Mouchet, A., Barriat, P.-Y., Campin, J.-M., Deleersnijder, E., Driesschaert, E., Goelzer, H., Haarsma, R., Janssens, Y., Loutre, M.-F., Maqueda, M.A.M., Opsteegh, T., Mathieu, P.-P., Munhoven, G., Petterson, E., Renssen, H., Roche, D., Schaeffer, M., Selten, F., Severijns, C., Tartinville, B., Weber, N., 2010. Description of the Earth system model of intermediate complexity LOVECLIM version 1.2. Geosci. Model Dev. 3, 603–633.

Griffies, S., 2012. Elements of the modular ocean model (MOM): 2012 release (GFDL ocean group technical report No. 7). Tech. rep. NOAA/Geophysical Fluid Dynamics Laboratory, Princeton, USA.

Griffies, S., Biastoch, A., Boning, C., Bryan, F., Danabasoglu, G., Chassignet, E., England, M., Gerdes, R., Haak, H., Hallberg, R., Hazeleger, W., Jungclaus, J., Large, W., Madec, G., Pirani, A., Samuels, B., Scheinert, M., Gupta, A.S., Severijns, C., Simmons, H., Treguier, A.M., Winton, M., Yeager, S., Yin, J., 2009. Coordinated Ocean–ice Reference Experiments (COREs). Ocean Model. 26, 1–46.

Grousset, F., Cortijo, E., Huon, S., Hervé, L., Richter, T., Burdloff, D., Duprat, J., Weber, O., 2001. Zooming in on Heinrich layers. Paleoceanography 16, 240–259.

Harrison, S., Sánchez Goñi, M., 2010. Global patterns of vegetation response to millennial-scale variability and rapid climate change during the last glacial period. Quat. Sci. Rev. 29, 2957–2980.

Hemming, S., 2004. Heinrich events: massive late Pleistocene detritus layers of the North Atlantic and their global climate imprint. Rev. Geophys. 42. 2003RG000128.

Huber, C., Leuenberger, M., Spahni, R., Flückiger, J., Schwander, J., Stocker, T., Johnsen, S., Landais, A., Jouzel, J., 2006. Isotope calibrated Greenland temperature record over Marine Isotope Stage 3 and its relation to CH4. Earth Planet. Sci. Lett. 243, 504–519.

Jouzel, J., Masson, V., Cattani, O., Dreyfus, G., Falourd, S., Hoffmann, G., Minster, B., Nouet, J., Barnola, J., Chappellaz, J., Fischer, H., Gallet, J., Leuenberger, S.J.M., Loulergue, L., Luethi, D., Oerter, H., Parrenin, F., Raisbeck, G., Raynaud, D., Schilt, A., Schwander, J., Selmo, E., Souchez, R., Spahni, R., Stauffer, B., Steffenssen, J.P., Stenni, B., Stocker, T., Tison, J., Werner, M., Wolff, E., 2007. Orbital and millennial Antarctic climate variability over the past 800,000 years. Science 317, 793–796.

Kageyama, M., Merkel, U., Otto-Bliesner, B., Prange, M., Abe-Ouchi, A., Lohmann, G., Roche, D., Singarayer, J., Swingedouw, D., Zhang, X., 2013. Climatic impacts of fresh water hosing under Last Glacial Maximum conditions: a multi-model study. Clim. Past 9, 935–953.

Kageyama, M., Mignot, J., Swingedouw, D., Marzin, C., Alkama, R., Marti, O., 2009. Glacial climate sensitivity to different states of the Atlantic Meridional Overturning Circulation: results from the IPSL model. Clim. Past 5, 551–570.

Kaiser, J., Lamy, F., Hebbeln, D., 2005. A 70-kyr sea surface temperature record off Southern Chile. Paleoceanography 20. http://dx.doi.org/10.1029/2004PA001146.

Key, R., Kozyr, A., Sabine, C., Lee, K., Wanninkhof, R., Bullister, J., Feely, R., Millero, F., Mordy, C., Peng, T.-H., 2004. A global ocean carbon climatology: results from GLODAP. Glob. Biogeochem. Cycles 18, GB4031.

Kissel, C., Laj, C., Piotrowski, A., Goldstein, S., Hemming, S., 2008. Millennial-scale propagation of Atlantic deep waters to the glacial Southern Ocean. Paleoceanography 23, PA2102.

Köhler, P., Joos, F., Gerber, S., Knutti, R., 2005. Simulated changes in vegetation distribution, land carbon storage, and atmospheric CO_2 in response to a collapse of the North Atlantic thermohaline circulation. Clim. Dyn. 25, 689–708.

Kwon, E., Primeau, F., Sarmiento, J., 2009. The impact of remineralization depth on the air–sea carbon balance. Nat. Geosci. 2, 630–635.

Kwon, E., Sarmiento, J., Toggweiler, J., DeVries, T., 2011. The control of atmospheric pCO_2 by ocean ventilation change: the effect of the oceanic storage of biogenic carbon. Glob. Biogeochem. Cycles 25. http://dx.doi.org/10.1029/2011GB004059.

Large, W., Yeager, S., 2009. The global climatology of an interannually varying air–sea flux data set. Clim. Dyn. 33, 341–364.

Lee, S.-Y., Chiang, J.C.H., Matsumoto, K., Tokos, K.S., 2011. Southern Ocean wind response to North Atlantic cooling and the rise in atmospheric CO_2: modeling perspective and paleoceanographic implications. Paleoceanography 26. http://dx.doi.org/10.1029/2010PA002004.

Lopes dos Santos, R., Spooner, M., Barrows, T., Deckker, P.D., Damsté, J.S., Schouten, S., 2013. Comparison of organic (UK37, TEXH 86, LDI) and faunal proxies (foraminiferal assemblages) for reconstruction of late Quaternary sea surface temperature variability from offshore southeastern Australia. Paleoceanography 28. http://dx.doi.org/10.1002/palo.20035.

Marchal, O., Stocker, T.F., Joos, F., Indermühle, A., Blunier, T., Tschumi, J., 1999. Modelling the concentration of atmospheric CO_2 during the Younger Dryas climate event. Clim. Dyn. 15, 341–354.

Marinov, I., Gnanadesikan, A., Toggweiler, J., Sarmiento, J., 2006. The Southern Ocean biogeochemical divide. Nature 441, 964–967.

Martrat, B., Grimalt, J., Shackleton, N., de Abreu, L., Hutterli, M., Stocker, T., 2007. Four climate cycles of recurring deep and surface water destabilizations on the Iberian margin. Science 317, 502–507.

Masson-Delmotte, V., Schulz, M., Abe-Ouchi, A., Beer, J., Ganopolski, A., González Rouco, J.F., Jansen, E., Lambeck, K., Luterbacher, J., Naish, T., Osborn, T., Otto-Bliesner, B., Quinn, T., Ramesh, R., Rojas, M., Shao, X., Timmermann, A., 2013. Information from paleoclimate archives. In: Stocker, T.F., Qin, D., Plattner, G.-K., Tignor, M., Allen, S.K., Boschung, J., Nauels, A., Xia, Y., Bex, V., Midgley, P.M. (Eds.), Climate Change 2013: The Physical Science Basis. Contribution of Working Group I to the Fifth Assessment Report of the Intergovernmental Panel on Climate Change. Cambridge Univ. Press, Cambridge, United Kingdom and New York, NY, USA, pp. 383–464.

Matsumoto, K., Yokoyama, Y., 2013. Atmospheric $\Delta^{14}C$ reduction in simulations of Atlantic overturning circulation shutdown. Glob. Biogeochem. Cycles 27. http://dx.doi.org/10.1002/gbc.20035.

Menviel, L., England, M., Meissner, K., Mouchet, A., Yu, J., 2014a. Atlantic–Pacific seesaw and its role in outgassing CO_2 during Heinrich events. Paleoceanography 29. http://dx.doi.org/10.1002/2013PA002542.

Menviel, L., Timmermann, A., Friedrich, T., England, M., 2014b. Hindcasting the continuum of Dansgaard–Oeschger variability: mechanisms, patterns and timing. Clim. Past 10, 63–77.

Menviel, L., Timmermann, A., Mouchet, A., Timm, O., 2008. Meridional reorganizations of marine and terrestrial productivity during Heinrich events. Paleoceanography 23, PA1203.

Morrison, A., Saenko, O., Hogg, A., Spence, P., 2013. The role of vertical eddy transport in Southern Ocean heat uptake. Geophys. Res. Lett. 40, 5445–5450.

Mouchet, A., 2011. A 3D model of ocean biogeochemical cycles and climate sensitivity studies. Ph.D. thesis. Université de Liège, Liège, Belgium. http://hdl.handle.net/2268/98995.

Obata, A., 2007. Climate–carbon cycle model response to freshwater discharge into the North Atlantic. J. Climate 20, 5962–5976.

Otto-Bliesner, B., Brady, E., 2010. The sensitivity of the climate response to the magnitude and location of freshwater forcing: last glacial maximum experiments. Quat. Sci. Rev. 29, 56–73.

Pahnke, K., Zahn, R., 2005. Southern Hemisphere water mass conversion linked with North Atlantic climate variability. Science 307, 1741–1746.

Pahnke, K., Zahn, R., Elderfield, H., Schulz, M., 2003. 340,000-year centennial-scale marine record of Southern Hemisphere climatic oscillation. Science 301, 948–952.

Parrenin, F., Barnola, J.-M., Beer, J., Blunier, T., Castellano, E., Chappellaz, J., Dreyfus, G., Fischer, H., Fujita, S., Jouzel, J., Kawamura, K., Lemieux-Dudon, B., Loulergue, L., Masson-Delmotte, V., Narcisi, B., Petit, J.-R., Raisbeck, G., Raynaud, D., Ruth, U., Schwander, J., Severi, M., Spahni, R., Steffensen, J.P., Svensson, A., Udisti, R., Waelbroeck, C., Wolff, E., 2007. The EDC3 chronology for the EPICA Dome C ice core. Clim. Past 3, 485–497.

Perez, R., Garzoli, S., Meinen, C., Matano, R., 2011. Geostrophic velocity measurement techniques for the meridional overturning circulation and meridional heat transport in the South Atlantic. J. Atmos. Ocean. Technol. 28, 1504–1521.

Richter, I., Xie, S.-P., 2010. Moisture transport from the Atlantic to the Pacific basin and its response to North Atlantic cooling and global warming. Clim. Dyn. 35, 551–566.

Roberts, W., Valdes, P., Payne, A., 2014. A new constraint on the size of Heinrich Events from an iceberg/sediment model. Earth Planet. Sci. Lett. 386, 1–9.

Röthlisberger, R., Mulvaney, R., Wolff, E., Hutterli, M., Bigler, M., Sommer, S., Jouzel, J., 2002. Dust and sea-salt variability in central East Antarctica (Dome C) over the last 45 kyrs and its implications for southern high-latitude climate. Geophys. Res. Lett. 29. http://dx.doi.org/10.1029/2002GL015186.

Sachs, J., Anderson, R., 2005. Increased productivity in the subantarctic ocean during Heinrich events. Nature 434, 1118–1121.

Sánchez-Goñi, M., Cacho, I., Turon, J.-L., Guiot, J., Sierro, F., Peypouquet, J.-P., Grimalt, J., Shackleton, N., 2002. Synchroneity between marine and terrestrial responses to millennial scale climatic variability during the last glacial period in the Mediterranean region. Clim. Dyn. 19, 95–105.

Sánchez-Goñi, M., Harrison, S., 2010. Millennial-scale climate variability and vegetation changes during the Last Glacial: concepts and terminology. Quat. Sci. Rev. 29, 2823–2827.

Sarmiento, J., Gruber, N., 2006. Ocean Biogeochemical Dynamics, vol. 526. Princeton University Press, Princeton, NJ.

Sarnthein, M., Stattegger, K., Dreger, D., Erlenkeuser, H., Grootes, P., Haupt, B., Jung, S., Kiefer, T., Kuhnt, W., Pflaumann, U., Schäfer-Neth, C., Schulz, H., Schulz, M., Seidov, D., Simstich, J., van Kreveld, S., Vogelsang, E., Völker, A., Weinelt, M., 2001. Fundamental modes and abrupt changes in North Atlantic circulation and climate over the last 60 ky – Concepts, reconstructions and numerical modeling. In: The Northern North Atlantic: A Changing Environment. Springer-Verlag, Berlin, pp. 365–410.

Schmittner, A., Brook, E., Ahn, J., 2007. Impact of the ocean's overturning circulation on atmospheric CO_2. In: Ocean Circulation: Mechanisms and Impacts. In: Geophysical Monograph Series, vol. 173. AGU, pp. 209–246.

Schmittner, A., Galbraith, E., 2008. Glacial greenhouse-gas fluctuations controlled by ocean circulation changes. Nature 456, 373–376.

Schmittner, A., Oschlies, A., Matthews, H., Galbraith, E., 2008. Future changes in climate, ocean circulation, ecosystems, and biogeochemical cycling simulated for a business-as-usual CO_2 emission scenario until year 4000 AD. Glob. Biogeochem. Cycles 22. http://dx.doi.org/10.1029/2007GB002953.

Scholze, M., Knorr, W., Heimann, M., 2003. Modelling terrestrial vegetation dynamics and carbon cycling for an abrupt climatic change event. Holocene 13, 327–333.

Sheen, K., Garabato, A.N., Brearley, J., Meredith, M., Polzin, K., Smeed, D., Forryan, A., King, B., Sallée, J., Laurent, L.S., Thurnherr, A., Toole, J., Waterman, S., Watson, A., 2014. Eddy-induced variability in Southern Ocean abyssal mixing on climatic timescales. Nat. Geosci.. http://dx.doi.org/10.1038/NGEO02200.

Spence, P., Dufour, C., Saenko, O., Sommer, J.L., England, M., 2012. Mechanisms maintaining Southern Ocean meridional heat transport under projected wind forcing. J. Phys. Oceanogr. 42, 1923–1931.

Spence, P., Sebille, E.V., Saenko, O., England, M., 2013. Using Eulerian and Lagrangian approaches to investigate wind-driven changes in the Southern Ocean abyssal circulation. J. Phys. Oceanogr. 44, 662–675.

Stocker, T., 1998. The seesaw effect. Science 282, 61–62.

Svensson, A., Andersen, K., Bigler, M., Clausen, H., Dahl-Jensen, D., Davies, S., Johnsen, S., Muscheler, R., Parrenin, F., Rasmussen, S., Röthlisberger, R., Seierstad, I., Steffensen, J., Vinther, B.M., 2008. A 60,000 year Greenland stratigraphic ice core chronology. Clim. Past 4, 47–57.

Takahashi, T., Olafsson, J., Goddard, J., Chipman, D., Sutherland, S., 1993. Seasonal-variation of CO_2 and nutrients in the high-latitude surface oceans – a comparative-study. Glob. Biogeochem. Cycles 7, 843–878.

Timm, O., Timmermann, A., Abe-Ouchi, A., Segawa, T., 2008. On the definition of paleo-seasons in transient climate simulations. Paleoceanography 23, PA2221. http://dx.doi.org/10.1029/2007PA001461.

Timmermann, A., Menviel, L., Okumura, Y., Schilla, A., Merkel, U., Hu, A., Otto-Bliesner, B., Schulz, M., 2010. Towards a quantitative understanding of millennial-scale Antarctic warming events. Quat. Sci. Rev. 29, 74–85.

Timmermann, A., Schulz, M., Gildor, H., Tziperman, E., 2003. Coherent resonant millennial-scale climate oscillations triggered by massive meltwater pulses. J. Climate 16, 2569–2585.

Uemura, R., Masson-Delmotte, V., Jouzel, J., Landais, A., Motoyama, H., Stenni, B., 2012. Ranges of moisture-source temperature estimated from Antarctic ice cores stable isotope records over glacial–interglacial cycles. Clim. Past 8, 1109–1125.

Volkov, D., Fu, L.-L., Lee, T., 2010. Mechanisms of the meridional heat transport in the Southern Ocean. Ocean Dyn. 60, 791–801.

Wang, Y., Cheng, H., Edwards, R., An, Z., Wu, J., Shen, C., Dorale, J., 2001. A high-resolution absolute-dated Late Pleistocene monsoon record from Hulu Cave, China. Science 294, 2345–2348.

Weaver, A., Eby, M., Wiebe, E., Bitz, C., Duffy, P., Ewen, T., Fanning, A., Holland, M., MacFadyen, A., Matthews, H., Meissner, K., Saenko, O., Schmittner, A., Wang, H., Yoshimori, M., 2001. The UVic Earth System Climate Model: model description, climatology, and applications to past, present and future climates. Atmos.-Ocean 4, 361–428.

Wunsch, C., 2007. The past and future ocean circulation from a contemporary perspective. In: Ocean Circulation: Mechanisms and Impacts. In: Geophysical Monograph Series, vol. 173. AGU.

Yu, J., Anderson, R., Jin, Z., Menviel, L., Zhang, F., Ryerson, F., Rohling, E., 2014. Deep South Atlantic carbonate chemistry and increased interocean deep water exchange during the last deglaciation. Quat. Sci. Rev. 90, 80–89.